Identification and Reduction of Interactional Noise of a Quadcopter in Hover and Forward Flight Conditions

Nikolas S. Zawodny[1]
Nicole A. Pettingill[2]
Christopher S. Thurman[3]
Aeroacoustics Branch
NASA Langley Research Center
Hampton, VA 23681

ABSTRACT

Advanced Air Mobility is a vision for a safe, accessible, and sustainable aviation system to transport people and cargo between places not served by traditional aviation. With this emerging transportation industry, there is motivation to characterize the noise of vehicles to determine their potential impacts on the community. An experimental testing campaign was conducted on a representative model of a small unmanned aircraft system in the NASA Langley Low Speed Aeroacoustic Wind Tunnel as a continuation of a previous testing campaign. The goals of the current test are to identify sources of interactional noise as well as to test custom-designed rotors and noise reduction devices. The tested noise reduction methods involve increasing the vertical distances between the rotors and the vehicle airframe as well as between the forward and aft rotor disk planes. These methods are intended to reduce rotor-airframe interaction noise in hover and fore-aft rotor wake ingestion noise in forward flight. A phased microphone array is also utilized to identify the locations of prominent noise generation for the different vehicle configurations in forward flight. Elevation of the rotors from the vehicle airframe yielded nearly 8 dBA overall noise reduction in forward flight, while yielding up to 4 dB reduction in overall tonal levels for one of the rotors in hover.

1. INTRODUCTION

Small Unmanned Aircraft Systems (sUAS) and Urban Air Mobility (UAM) aircraft are key components of the emerging Advanced Air Mobility (AAM) aviation industry. UAM aircraft are planned to perform passenger transport missions up to 120 km (75 miles) around metropolitan areas, while sUAS vehicles are expected to perform local missions including aerial imaging and small cargo delivery. [1] One aircraft configuration that is common to both of these vehicle classes is the multicopter. An overwhelming majority of sUAS that have been documented by the FAA are of the multicopter variety.In addition, the NASA Revolutionary Vertical Lift Technology (RVLT) project has overseen the development of a range of UAM vehicle concepts, including a six-passenger quadrotor vehicle. [2] Furthermore, previous experimental investigations have found that sUAS vehicle sounds can be more annoying than similar amplitude sounds generated by ground vehicles. [3, 4] Therefore, characterization of the noise sources of these vehicles is important so that noise reduction opportunities can be identified and implemented.

[1]nikolas.s.zawodny@nasa.gov

[2]nicole.a.pettingill@nasa.gov

[3]christopher.thurman@nasa.gov

Previous experimental testing of a quadcopter in an acoustic wind tunnel environment revealed vehicle performance and acoustic data that agreed well with flight test measurements of the same nominal vehicle. [4, 5] This prior investigation identified noise characteristics in both hover and forward flight that were believed to originate as a result of complex aerodynamic interaction mechanisms. Specifically, these mechanisms included tonal harmonic excitations in hover believed to be due to rotor-airframe interactions, [6] as well as considerable increases in broadband noise for fore-aft rotor pairs operating in forward flight believed to be due to front rotor wake ingestion by the aft rotor. [7] The current testing campaign seeks to identify these noise source mechanisms and implement rudimentary noise reduction mechanisms.

2. TECHNICAL APPROACH

2.1. Facility and Test Setups

The Low Speed Aeroacoustic Wind Tunnel (LSAWT) is an open-circuit free jet wind tunnel that is currently configured for a freestream Mach number range of $0.045 \leq M_\infty \leq 0.143$ and is reconfigurable to an upper end capability of $M_{\infty,\max} = 0.32$. More details of the facility capabilities can be found in Reference 8. A summary of the test setup is depicted in Figure 1. As shown in

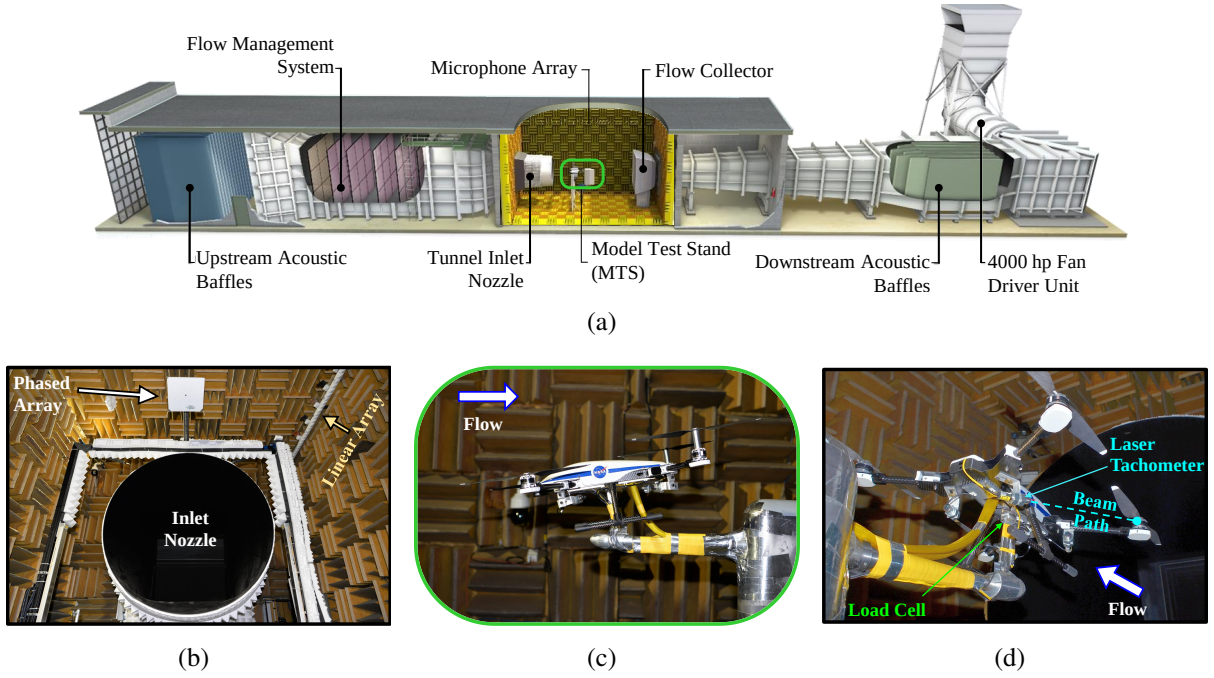

Figure 1: LSAWT and model test stand setups: (a) Rendered cut-away illustration of the LSAWT, (b) phased and linear microphone arrays, (c) quadcopter mounted on the MTS, (d) on-vehicle measurement devices.

Figure 1(a), the anechoic test chamber is centrally located along the length of the facility, and it is acoustically treated with fiberglass wedges down to a cut-off frequency of approximately 250 Hz. Two acoustic arrays were utilized in this study: a streamwise linear array of 28 B&K type 4939 free-field microphones, and a commercially available phased microphone array (OptiNav ACAM 120). As shown in Figure 1(b), the linear microphone array is located along one of the facility upper corners in the streamwise direction, and the phased array is in an overhead position, just outside of the tunnel shear layer. The purpose of the linear array is to gather acoustic spectra and directivity information, while the phased array allows for noise source localization via beamforming. Figures 1(c) and 1(d) provide close-up views of the quadcopter installed on the LSAWT model test stand (MTS). Figure 1(d) shows the on-vehicle measurement instrumentation as well, which consist of an ATI-IA Mini40 multiaxis load cell and a total of four laser tachometers (one for each rotor) for

tracking motor rotation speeds, all located on the underside of the vehicle airframe. More details of this instrumentation can be found in Reference 5.

The test article in this study is the same Straight Up Imaging (SUI) Endurance quadcopter model hardware tested in References 5 and 7. A rendered planform view of the vehicle is provided in Figure 2. The primary components of the vehicle include a faired airframe, four rotors, and a landing gear assembly. The vehicle's forward rotors are herein referred to as R1 and R2, while the aft rotors are referred to as R3 and R4. The rotational sense of each rotor is such that it is counter-rotating relative to its neighboring rotors. The hub-to-hub distance between neighboring motors is approximately 510 mm (≈20 in.). Each rotor consists of two carbon fiber fixed-pitch blades, each with a blade radius of $R = 190.5$ mm (7.5 in.). More details of the SUI Endurance vehicle model can be found in References 5 and 7.

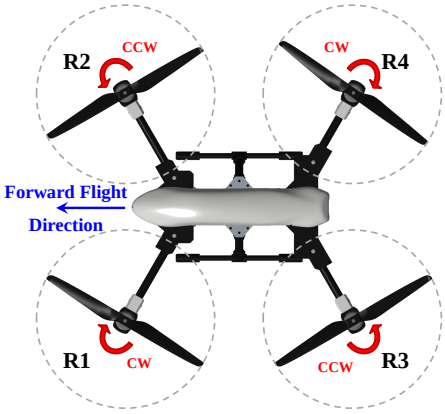

Figure 2: SUI Endurance quadcopter with rotor nomenclature.

Figure 3 provides upstream and sideline sketches of the linear and phased microphone array locations and orientations relative to the quadcopter model. As Figure 3(a) shows, the linear

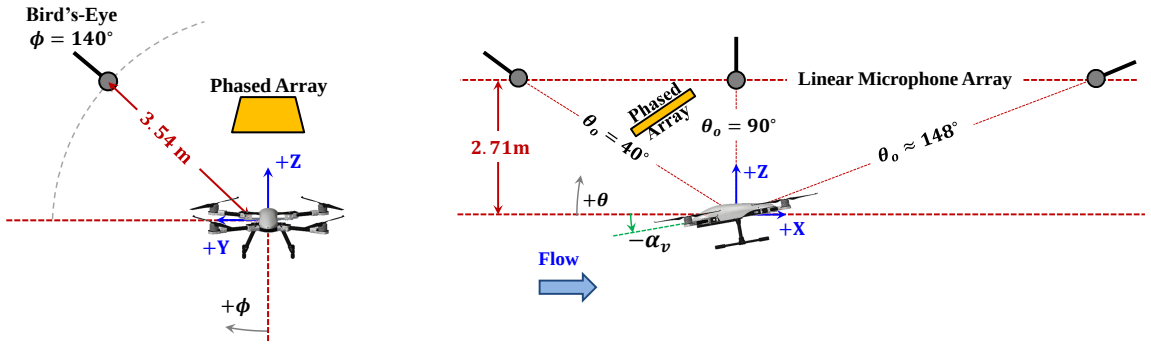

(a) Upstream view

(b) Profile view

Figure 3: Linear and phased microphone array locations: (a) upstream view of azimuthal plane (flow is into page), (b) profile view of polar plane (bird's-eye configuration). (Note: images not drawn to scale)

microphone array was at an azimuthal angle of $\phi = 140°$ relative to the underside of the vehicle model. This "bird's eye" view acoustic survey of the vehicle was one of four acoustic survey orientations performed in Reference 5, which were attainable by rotating the vehicle about the MTS. Only data for the bird's eye orientation were acquired in this study due to the numerous vehicle configurations tested as well as the structural risk imposed to the model hardware and MTS by some of the tested configurations. This acoustic survey orientation was deemed appropriate to assess representative changes in vehicle acoustics associated with vehicle configurations, based on very similar directivity characteristics previously measured between the bird's eye and flyover microphone survey orientations. [5] The phased microphone array was positioned just outside of the LSAWT open-jet shear layer in an overhead position relative to the vehicle. This location was chosen due to the fact that rotor broadband noise tends to exhibit maximum acoustic levels out-of-plane of the rotors, [9] as well as to provide unobstructed views of the entire vehicle. The phased array was positioned 1.26 m (49.5 in.) away from the model center and was only present for forward flight conditions.

2.2. Flight Conditions and Vehicle Configurations

Similar to Reference 5, the vehicle was dynamically trimmed for a low, middle, and high thrust condition (27, 36, and 45 N) for both hover and forward flight conditions. Several forward flight

velocities and vehicle forward pitch angles were implemented in an effort to emulate a range of advance ratios representative of both UAS and UAM flight vehicles. Noise mitigation strategies were also tested and included rotor elevation standoffs of two different lengths (short and tall), as well as a custom-designed and custom-fabricated set of rotor blades. A pictorial summary of the vehicle configurations tested in this study is provided in Figure 4. The motivations behind testing elevation

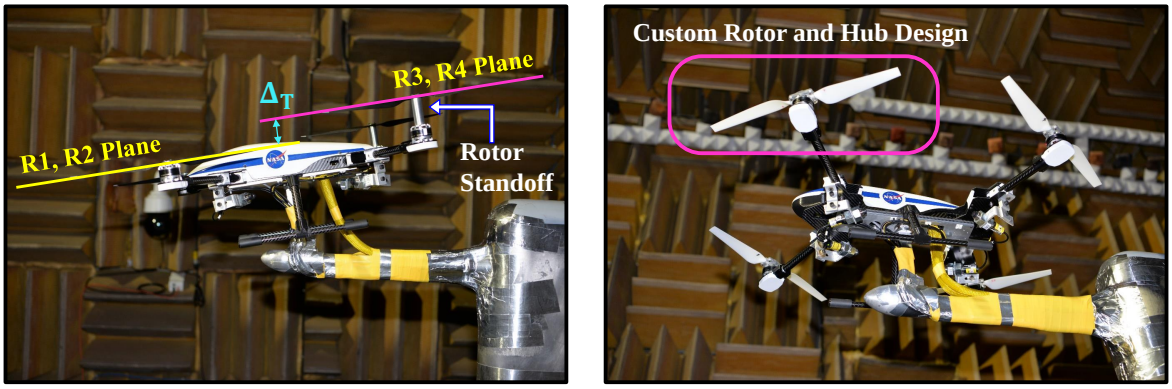

(a) Elevated Rotors (b) Custom Rotor Assemblies

Figure 4: Summary of tested vehicle configurations in the current study.

standoffs are twofold: (1) reduce rotor-airframe interaction noise in hover conditions by reducing the impulsive rotor downwash effect on the airframe [6] and (2) reduce forward flight interaction noise due to front rotor wake and airframe wake ingestion into the aft rotor disks [5,7,10]. Furthermore, there are multiple motivations behind testing custom rotor designs, including reduction of rotor self-noise and assessments of the effects of different blade pitch settings. This study focuses on the effects of the rotor elevation on interactional noise, while the results of the custom rotors are provided in a companion publication [11]. The two rotor elevation standoff distances tested are $\Delta_S = 32$mm $(0.17R)$ and $\Delta_T = 64$mm $(0.33R)$ relative to their baseline plane of rotation, which represent the *short* and *tall* elevation heights, respectively. A summary of test conditions for investigating interactional noise are provided in Table 1. As this table shows, hover measurements were performed at a vehicle pitch angle of $\alpha_v = 0°$, while forward flight conditions were conducted at angles of $\alpha_v = -10°$ and $-4°$. The former of these settings was tested in Reference 5, while the latter one was tested in an effort to better align with existing flight test data [4] as well as to better represent UAM vehicle configurations [2]. All full vehicle configuration tests were run with all rotors in simultaneous operation until the vehicle was trimmed to the target thrust condition. These trim conditions were determined such that the pitch, roll, and yaw moments were nearly zero and the desired net thrust condition was achieved. It is important to note that these trimmed conditions do not fully account for the drag loads encountered by the vehicle in forward flight. The combined conditions that were found to most closely represent the vehicle in steady level flight were those at a freestream condition of $M_\infty = 0.046$, $\alpha_v = -10°$, and the high thrust condition. Similar to Reference 5, rotors R1 and R3 were run individually for all tested configurations, while the simultaneous operation of R1 and R3 was performed for all forward flight conditions. Only the low thrust setting was tested for the higher flow speed due to structural limitations of the vehicle and test stand.

2.3. Data Acquisition and Processing

Dynamic data were acquired on National Instruments^{TM} dynamic signal acquisition modules installed in a PXIe-1085 chassis. Microphone data were acquired on several PXIe 4480 modules at a sampling rate of 102.4 kHz, while load cell data were acquired on a single PXI 6143 module at a lower sampling rate of 80 kHz. Microphone and vehicle performance data acquisitions were divided between these two module types to allow for real-time monitoring of the performance data to establish vehicle trim conditions. Microphone data were high-pass filtered at 10 Hz, which provided a usable flat passband (less than -0.5 dB deviation) within a frequency range of 50 Hz $\leq f \leq$ 40

Table 1: Experimental testing conditions for investigating interactional noise.

Flow Speed	**Vehicle Thrust**			**Vehicle Pitch**			**Rotor Elevations**[1]		
M_∞	Low	Mid	High	0°	−4°	−10°	Fwd Only	Aft Only	Fwd + Aft[4]
0.0 (Hover)[2]	✓	✓	✓	✓	✗	✗	Tall	Tall	Tall
0.046 (UAS)[3]	✓	✓	✓	✗	✓	✓	✗	Short, Tall	Tall
0.065 (UAM)[3]	✓	✗	✗	✗	✓	✓	✗	Tall	✗

[1]Nonelevated rotors (baseline) operated for every flight condition
[2]Rotor operations: All rotors simultaneously, R1 only, R3 only
[3]Rotor operations: All rotors simultaneously, R1 only, R3 only, R1 and R3 simultaneously
[4]Cases of forward and aft rotors elevated simultaneously not performed for $\alpha_v = -4°$

kHz. Load cell data were low-pass filtered at 32 kHz and DC-coupled to allow for steady load measurements. Filter and channel gain settings were implemented by running the microphone and load cell channels through a Precision Filter 28000 series chassis. Each wind tunnel run was acquired for a time duration of 20 seconds.

Acoustic data were processed using three different techniques. [5, 6, 9] The first and simplest of these is the narrowband spectrum, which is computed using the Fast Fourier Transform (FFT) using a Hanning window with 75% overlap and a frequency resolution of 10 Hz. The second allows for the separation of periodic and random noise components in the time domain by computing a mean rotor revolution time history, repeating it, then subtracting it from the original time record. This provides both a nominally *periodic* and *residual* time history, which can then be converted into the frequency domain using the first processing method. The third method involves narrow band-pass filtering of acoustic time series to retain only harmonics of the rotor blade passage frequency (BPF). Finally, three acoustic metrics are used in this study for both comparisons between flight conditions and between periodic and broadband noise contributions. They are the sound pressure level (SPL) spectrum, the overall sound pressure level (OASPL) denoted by L, and the A-weighted OASPL denoted by L_A. All OASPLs are calculated over a frequency range of $100 \leq f \leq 20,000$ Hz unless indicated otherwise. In addition to narrowband spectra as discussed previously, some spectra will also be presented in one-third octave bands ($SPL_{1/3}$) for visual clarity of trends.

3. RESULTS AND INTERPRETATION

3.1. Hover Acoustics

The acoustics of a rotor (or rotors) in hover can be difficult to measure in an enclosed or partially enclosed acoustically treated facility. [12] The onset of flow recirculation from rotor downwash and flow perturbations from the outside environment promotes the ingestion of turbulent structures back into the rotor disk area, which then results in rotor harmonic excitation and potential variation in rotor rotation rate. These chaotic effects can make comparisons with notional computational predictions difficult. However, recent work has also shown that these effects in an enclosed environment can emulate the turbulent atmosphere encountered by UAS rotors flown in an outside environment. [13] In the current study, hover data were acquired during both a dynamic ramp-up of rotor speed to a set condition, followed by an additional acquisition of the same target condition to identify rotor inflow perturbation effects. Due to a combination of quick onset of recirculation in the test cell as well as the fact that each motor was controlled manually, full vehicle operation at a constant thrust condition was very challenging. The resulting recirculation caused by all rotors in simultaneous operation could be quite considerable at times, making it difficult to perform comparisons between the different tested vehicle configurations. Therefore, only results for single rotor operation cases are presented here, specifically the operation of R3. Data were interrogated for a full 20 seconds after the motor ramp-up data run. This was done in an effort to yield results that could represent a realistic comparison

between vehicle configurations subject to a turbulent environment, and to not limit the analysis to an ideal measurement.

Figure 5 shows the changes in narrowband acoustic spectra and periodic-extracted tonal harmonics for single rotor operation. Figure 5(a) provides a spectral comparison between baseline and elevated

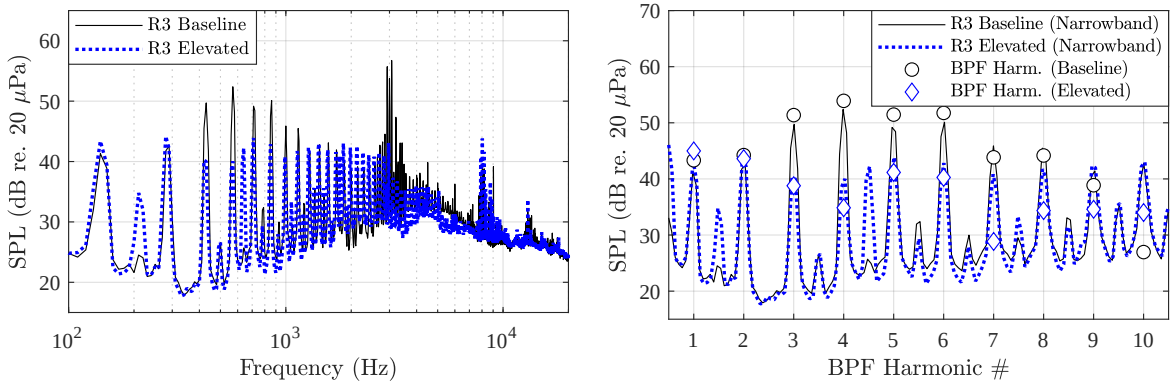

(a) R3 Narrowband Spectra (b) R3 BPF Harmonics

Figure 5: Impacts of rotor elevation on hover acoustic spectra. Note: data are at $\theta_o = 90°$ and for the medium thrust condition, $\overline{M_{tip}} = 0.24$.

rotor conditions for R3 operation at medium thrust. The results show prominent tonal harmonic content in the frequency range of 400 Hz $\leq f \leq$ 1 kHz for the baseline operation case, which is indicative of rotor-airframe interactions. [6] Figure 5(b) provides a closer examination of these harmonics plotted as multiples of the rotor BPF. This figure shows both narrowband as well as tone levels computed using the periodic extraction technique mentioned previously. The results show overall reasonable agreement between both the narrowband and periodic-extracted levels, however not exact for all harmonics. This is due to the presence of turbulent gusts that can promote random excitation at these frequencies, which are not retained in the periodic averaging process. There is considerable reduction in the levels of BPF harmonics 3-8 for the elevated rotor case using both metrics. There is also some additional energy in several of the intermediate tones - BPF harmonics 1.5 and 4.5 most notably - which is due to structural vibrations of the vehicle as a result of the installation of the rotor elevation standoffs.

Figure 6 shows the change in OASPL directivities between rotor elevation configurations for R3 operation cases. It is important to note that the OASPLs are computed over a frequency range of

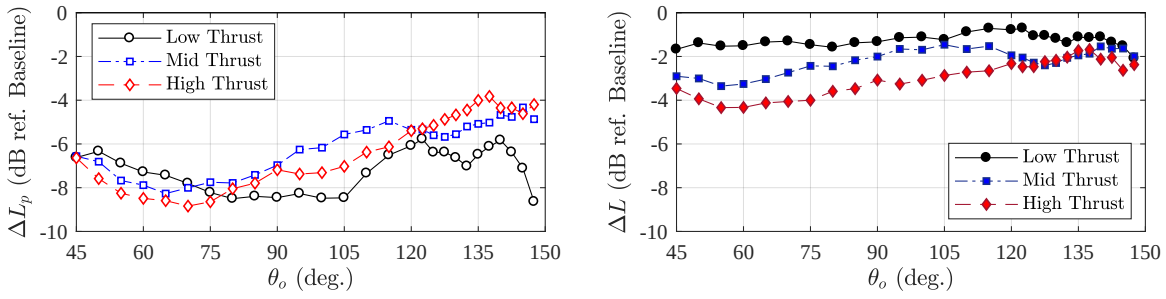

(a) Periodic Averaged Level Integration (b) Narrowband Integration

Figure 6: Impacts of R3 rotor elevation on hover acoustic OASPL directivity. Note that average rotor tip speeds for the low, medium, and high thrust conditions are $\overline{M_{tip}} = 0.21$, 0.24, and 0.27, respectively. OASPL data are integrated over 100 Hz $\leq f \leq$ 2.5 kHz, and indicated level differences are relative to the baseline rotor operation configuration.

100 Hz $\leq f \leq$ 2.5 kHz for all cases. This frequency range was chosen based on the presence of prominent motor noise for some configurations that could yield misleading comparative results if included in the integration. An example of such motor noise is visible in Figure 5(a) centered around 3, 8, and 12 kHz. This frequency range was deemed to be appropriate, however, based on the fact that the harmonic amplitudes begin to roll off around 1.5 kHz. Figure 6(a) shows between 4 and 8.5

dB integrated level reduction across the range of tested observer angles, when based on the periodic-extracted tonal amplitudes. This noise reduction benefit is seen to reduce to between 1 and 4 dB, however, in Figure 6(b) when the integration is performed on the narrowband spectral levels. The differences between these two figures are due to the simulated atmospheric turbulence generated due to flow recirculation in the facility, which is not retained in the data processing leading to Figure 6(a). While the results of the full vehicle operation cases are not shown here, elevation of the vehicle rotors yielded anywhere between a -3.0 dB integrated level reduction and a +1.3 dB integrated level increase depending on thrust setting and having the aft or all of the rotors elevated. A combination of factors are believed to contribute to a slight increase in noise; these include additional harmonic excitations due to structural vibrations associated with the rotor standoffs, varying thrust levels as a result of recirculation, and different phase relationships between the rotors across the different configuration runs. Therefore, while some noise reduction benefits are observed in these data, it is believed that real-world vehicle flight tests would need to be performed to statistically determine the benefits, if any, over a range of atmospheric conditions.

3.2. Forward Flight Acoustics

As was discussed in Section 2.2, the vehicle was operated in forward flight over several combinations of thrust, flight speed, vehicle pitch, and rotor elevation conditions. The following sections address the impacts of these different operational parameters on the radiated vehicle acoustics. Acoustic trends observed for the full vehicle operation cases are analyzed first, which are then followed by a more detailed analysis of the periodic and broadband noise contributions for the different configurations. More detailed results on these trends, as well as those observed for the vehicle operating at higher flow speeds, will be presented in a future publication.

3.2.1. Rotor Elevation Impacts on Full Vehicle Acoustics

A summary of key impacts of the elevation of the vehicle rotors on forward flight acoustics is provided in Figure 7. Figures 7(a) and 7(b) provide narrowband and one-third octave band

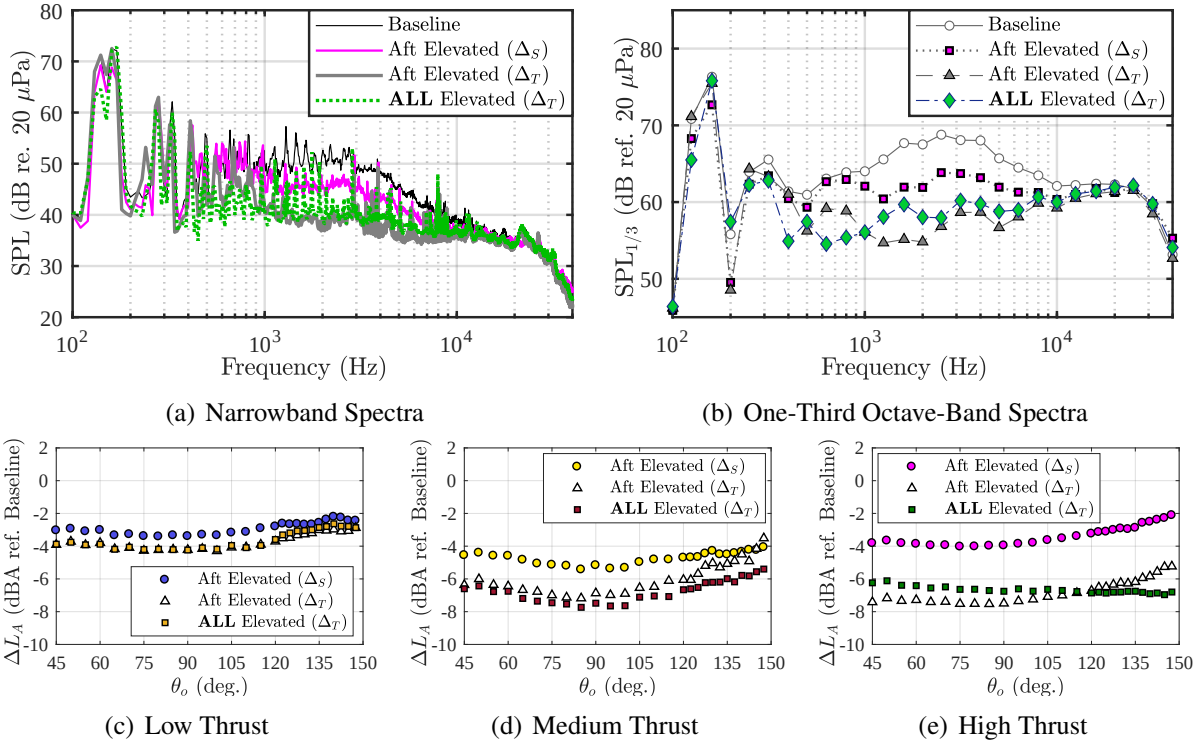

(a) Narrowband Spectra (b) One-Third Octave-Band Spectra

(c) Low Thrust (d) Medium Thrust (e) High Thrust

Figure 7: Impacts of rotor elevations on full vehicle forward flight acoustics. Data in (a) and (b) represent the high thrust condition at $\theta_o = 90°$. Data in (c) - (e) are relative to the baseline configuration directivities. Forward flight conditions: $M_\infty = 0.046$, $\alpha_v = -10°$.

representations of the full vehicle in operation for the high thrust condition at $\theta_o = 90°$, respectively. The narrowband data in Figure 7(a) are useful in how they provide a detailed view of the combination of tonal and broadband noise for the different rotor elevation conditions. In particular, the lowest frequency tones centered at 140 and 160 Hz represent the BPFs of the front and aft rotors, respectively, with some higher BPF harmonics visible at lower levels. Figure 7(b) is more useful for visualizing the changes in noise trends with rotor elevation conditions. This figure shows a gradual decrease in broadband noise centered around 2.5 kHz with increasing aft rotor elevation height. This provides evidence that this mid-frequency broadband noise is due to a wake ingestion phenomenon into the aft rotor disk areas, which is effectively mitigated as the aft rotors are elevated away from the front rotor planes and vehicle airframe. Furthermore, it is interesting to observe how the broadband noise for the case of all rotors elevated remains very similar to the case of only aft rotors elevated, with the exception of some additional mid-frequency tonal energy centered around 1.6 kHz, believed to be due to structural vibrations on the vehicle. This is a very important result because it indicates that returning the rotors to a common plane with each other did not cause the interactional broadband noise to return. This implies that the interactional broadband noise that is present for the baseline vehicle configuration is not solely caused by front rotor wake ingestion into the aft rotor system. Rather, it is caused by the interaction and energizing of the front rotor wake as the blade traverses over the airframe, which then interacts with the aft rotor system. Figures 7(c) - 7(e) provide the changes in A-weighted OASPL directivities with rotor elevations for the different vehicle thrust conditions. These results show consistent increasing noise reduction with increasing aft rotor elevation height for all tested thrust conditions, albeit at different levels. The results also show comparable noise reduction benefits for the cases of having all rotors elevated.

Figure 8 provides a summary of aft rotor elevation impacts on full vehicle acoustics at a vehicle pitch of $\alpha_v = -4°$. These data show an overall reduction in noise benefit when compared to the data previously shown for the $\alpha_v = -10°$ vehicle conditions. These data also show a decrease in noise benefit with increasing vehicle thrust level, which is opposite of the thrust trends previously shown in Figures 7(c) - 7(e). More information on this behavior can be ascertained by analyzing R1-R3 rotor pair operation cases in the next section.

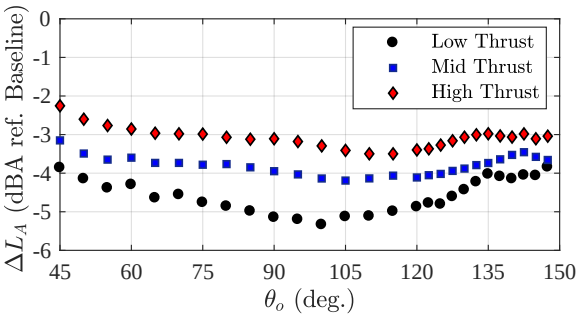

Figure 8: Aft rotor elevation (Δ_T) impacts on integrated levels for $\alpha_v = -4°$.

3.2.2. Periodic and Broadband Noise Contributions

Limiting the vehicle operation condition to simultaneous and individual operations of a forward and aft rotor pair - in this case, R1 and R3 - allows one to interrogate the unique tonal and broadband noise contributions that are due to aerodynamic interactions. Using the periodic extraction method discussed previously, the tonal and broadband noise components were differentiated for the cases of individual R1 or R3 operations, as well as for the cases of simultaneous rotor operations (R1 & R3). Figure 9 shows the periodic and broadband contributions of the R1 & R3 simultaneous operation case in forward flight at $M_\infty = 0.046$ and $\alpha_v = -10°$ for the baseline and R3 elevated conditions. The results of Figure 9(a) show a decrease in both periodic levels between 500 Hz and 2.5 kHz and broadband levels between 1 kHz and 10 kHz, with the broadband levels decreasing most prominently over the majority of measured observer angles in Figure 9(b). It is worth noting that similar decreases in periodic and broadband noise were found in cases where both rotors were elevated. It is also interesting to note how the results of Figure 9(b) show that the difference between periodic noise levels and broadband noise levels decreases when the the aft rotor is elevated, though the broadband noise contribution still dominates at all observers. While the data for $\alpha_v = -4°$ are not shown here, they display similar behaviors.

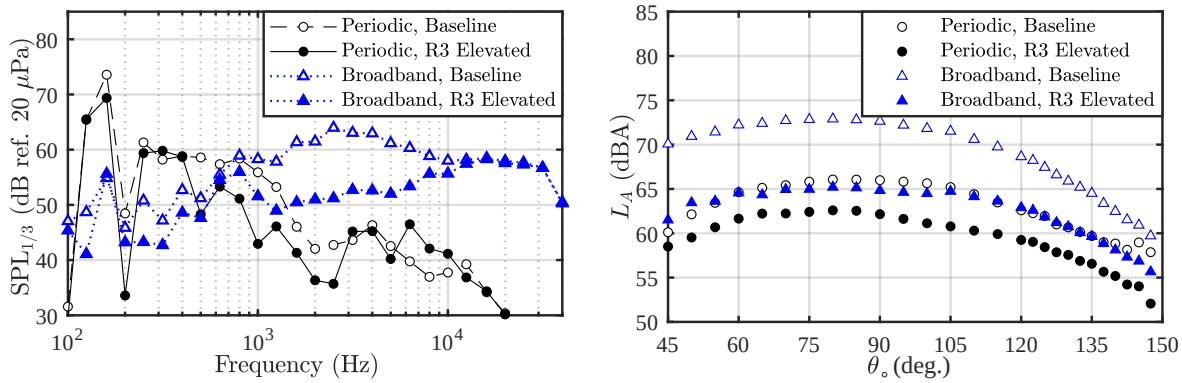

(a) Spectra at $\theta_o = 90°$ (b) L_A directivities

Figure 9: Impacts of aft rotor elevation (Δ_T) on R1 & R3 rotor pair forward flight extracted periodic and broadband noise for the high thrust condition and $\alpha_v = -10°$.

Figure 10 provides the broadband-extracted one-third octave spectra of the baseline and aft-elevated vehicle configurations for vehicle pitch angles of $\alpha_v = -10°$ and $-4°$. The figures include

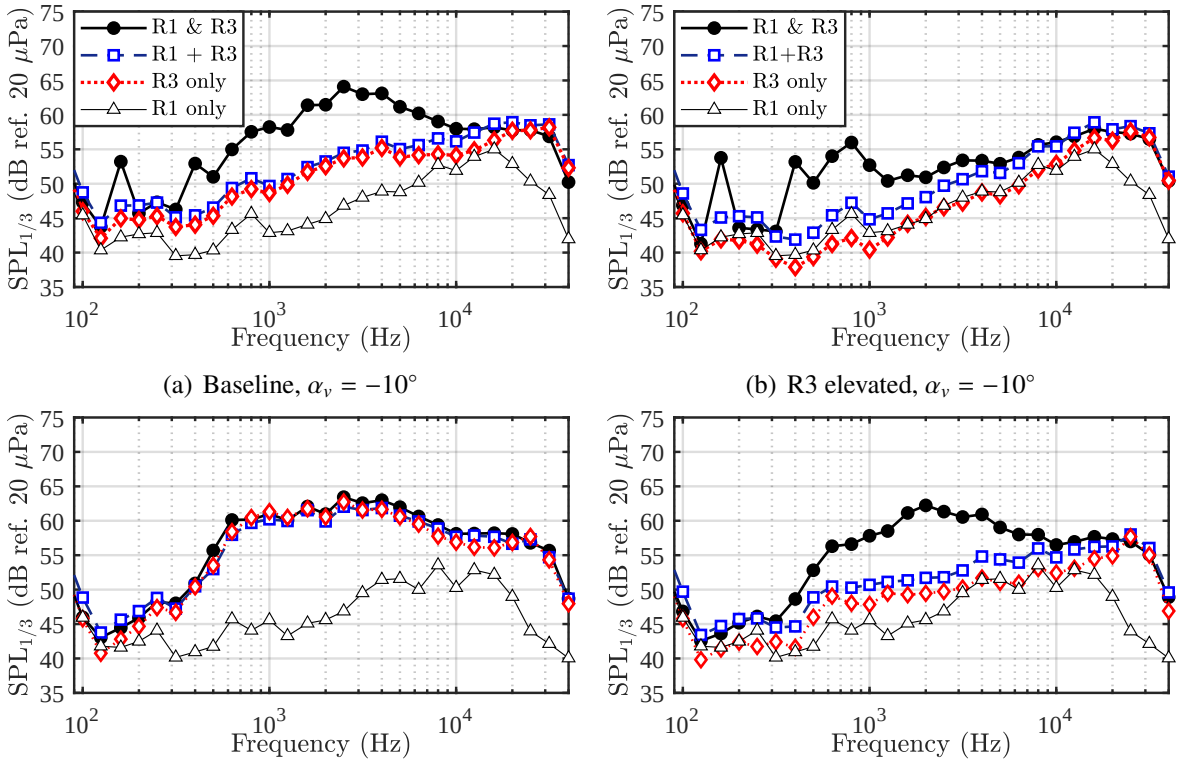

(a) Baseline, $\alpha_v = -10°$ (b) R3 elevated, $\alpha_v = -10°$

(c) Baseline, $\alpha_v = -4°$ (d) R3 elevated, $\alpha_v = -4°$

Figure 10: Impacts of aft rotor elevation (Δ_T) on R1 & R3 rotor pair forward flight extracted broadband noise for the high thrust condition at $M_\infty = 0.046$. Data shown are at $\theta_o = 90°$.

the measurements of rotors in simultaneous operation, individual operation, and the incoherent summation of the individual operation cases. Figure 10(a) shows that the case of simultaneous rotor operation exhibits considerably higher mid-frequency broadband noise levels than the individual rotor summation case. This figure also shows that R3 generates considerably more broadband noise when operated individually as compared to R1. Figure 10(b) shows the considerable reduction in mid-frequency broadband noise due to the elevation of R3, as well as a considerable reduction in individual R3 operation broadband noise. This implies that even when operated individually, the aft rotor experiences some level of wake interactions from the front rotor strut in the baseline configuration. Figure 10(c) is very interesting in that it shows nearly identical spectra for the cases of simultaneous rotors and R3 only operation cases for the vehicle at $\alpha_v = -4°$. This implies that the increase in broadband noise for this vehicle pitch orientation is almost solely due to airframe

wake ingestion into the aft rotor, regardless of whether or not the front rotor is operating. When the aft rotor is elevated, however, the operation of R3 individually yields much lower broadband noise levels, as indicated in Figure 10(d). This implies that the aft rotor was moved further outside of the airframe wake trajectory. This figure also shows that the simultaneous rotor operation case yet again results in an increase in mid-frequency broadband noise, which points to the front rotor wake as the cause. These results corroborate the change in the full vehicle integrated levels of Figure 8, indicating that an increase in vehicle thrust reduces the effectiveness of aft rotor elevation at reducing the mid-frequency broadband noise for this vehicle pitch condition, which is most likely due to the increase in front rotor wake velocities encountered by the aft rotor. This behavior resembles that of the baseline vehicle configuration at $\alpha_v = -10°$, which exhibits an increase in mid-frequency broadband interaction noise with increasing thrust condition [7].

3.2.3. Beamforming

To gain additional insight into the sources of noise for the different vehicle conditions, beamforming is implemented using the phased array discussed in Section 2.1 for the R1 & R3 rotor pair operation cases. Figure 11 provides a sample beamforming image at the 16 kHz one-third octave band center frequency for the baseline vehicle configuration operating at the high thrust condition for $M_\infty = 0.046$ and $\alpha_v = -10°$. As this image shows, there are comparable levels of noise being generated by both rotors at this frequency, with R1 generating slightly more noise. This source distribution is indicative of rotor self-noise, with the highest source intensity indicated on the advancing sides of the rotor blades. [7] This source distribution was found to be common for all tested vehicle configurations in this frequency range, which is also indicated by the similar noise levels of the configurations shown in Figures 7 and 10.

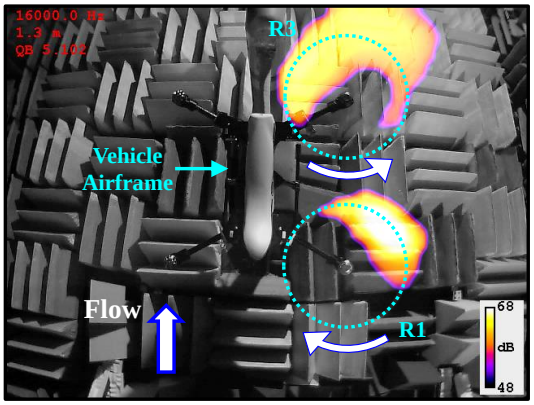

Figure 11: Sample beamforming image of baseline vehicle at $M_\infty = 0.046$ and $\alpha_v = -10°$. $F_c = 16$ kHz.

Figure 12 provides the beamforming images at a one-third octave center frequency of $F_c = 3.15$ kHz for the operating conditions shown previously in Figure 10. Note that this frequency range was selected for interrogation both because it represents a frequency at which the interactional broadband noise is near maximal, and due to the fact that it is in the range of highest human hearing sensitivity. Figure 12(a) shows a single region of high intensity noise on the advancing side of R3, in close proximity to the rotor strut-airframe junction. This is believed to be associated with the impingement of the combined wakes from the upstream forward rotor and its strut-airframe junction. This noise region is seen to disappear with the elevation of R3 in Figure 12(b) and is replaced by lower amplitude noise of comparable levels from both rotors. This corresponds to a nearly 10 dB drop in broadband noise level at this frequency previously shown in Figure 9(a). Figure 12(c) shows a very similar noise source distribution as Figure 12(a) at $\alpha_v = -4°$, while elevation of R3 is seen to only shift the dominant noise source downstream and provide a slight level reduction in Figure 12(d). This vehicle flight condition corresponds to only a 2 dB reduction in broadband noise level at this frequency in Figure 10(d). These results clearly indicate a dependency of rotor elevation from the airframe as an effective wake ingestion noise reduction method on a variety of parameters including thrust setting, upstream airframe geometry, and vehicle pitch orientation.

4. CONCLUSIONS

This study investigates the sources of noise caused by aerodynamic interactions on a representative multicopter system in simulated hover and forward flight conditions in an acoustic wind tunnel. This investigation is a continuation of a previous study in which general acoustic characteristics of this

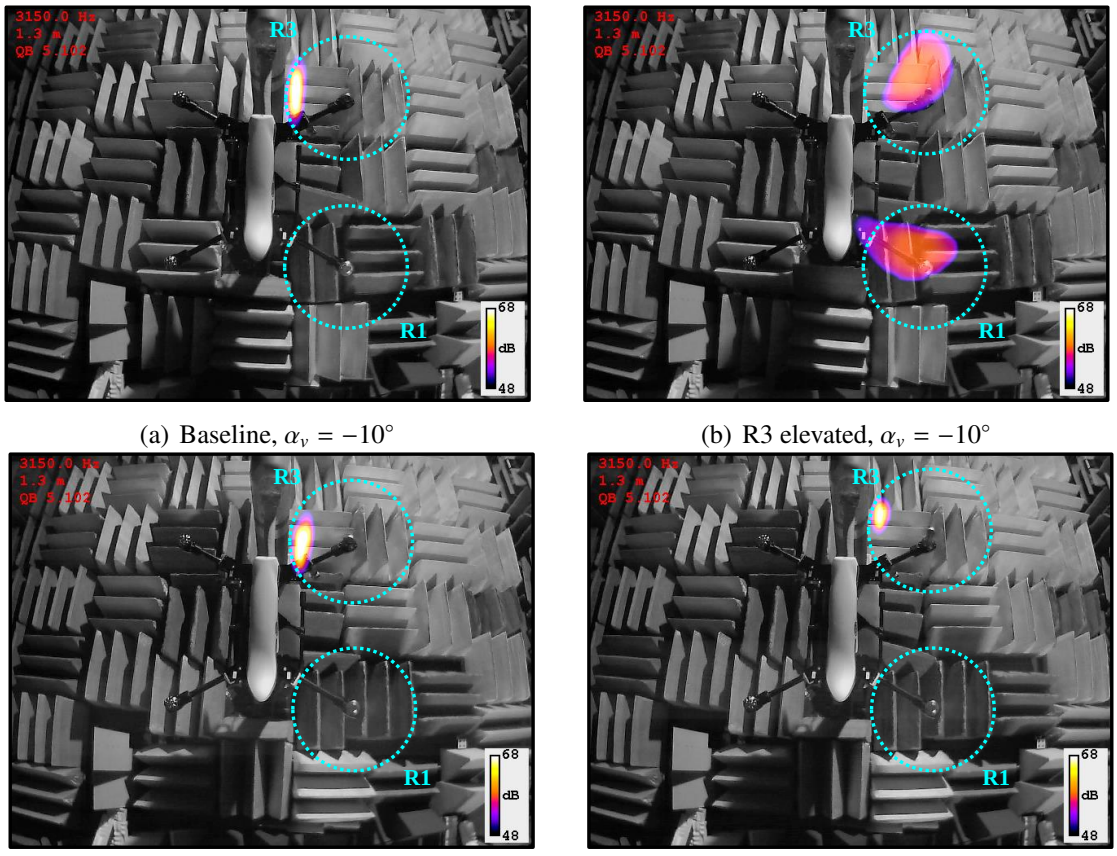

(a) Baseline, $\alpha_v = -10°$

(b) R3 elevated, $\alpha_v = -10°$

(c) Baseline, $\alpha_v = -4°$

(d) R3 elevated, $\alpha_v = -4°$

Figure 12: Impacts of aft rotor elevation on R1 & R3 rotor pair forward flight beamforming maps at F_c = 3.15 kHz. Images complement the data and conditions of Figure 10.

same vehicle were identified. The results of this previous investigation provided evidence of rotor-airframe interactions in hover and rotor-airframe wake interaction noise in forward flight. Therefore, different combinations of rotors were elevated above the airframe using hub standoffs to see if these interaction noise mechanisms could be reduced. As was found in the previous study, full vehicle operations in hover in the enclosed anechoic environment were very challenging. Elevation of a single rotor above the airframe yielded up to a 4 dB reduction in integrated narrowband acoustic levels, while the relatively fast onset of recirculation and unstable operating conditions for full vehicle operations made the results inconclusive. Elevation of the vehicle aft rotors was found to reduce interactional broadband noise as well as tonal noise in forward flight to varying extents depending on vehicle thrust and pitch settings. An A-weighted OASPL reduction between 4 and 8 dBA was observed between low and high thrust settings for the vehicle at a -10 degree vehicle pitch angle, and between a 3.5 and 5 dBA reduction between high and low thrust settings at the shallower -4 degree vehicle pitch angle. Beamforming provided visualizations of the dominant noise sources for the different tested configurations. The baseline vehicle configurations yielded a single concentrated source region coinciding with the aft rotor approaching the aft strut-airframe junction. This source is believed to coincide with the impingement of the upstream airframe and rotor wakes. While this source mechanism disappeared with aft rotor elevation for the steeper vehicle pitch configuration, it was only slightly reduced and shifted further downstream for the shallower pitch case. It is believed that the wakes generated by the front rotors can act as either a deflection or strengthening mechanism for the wakes generated by the vehicle airframe, and the resulting wake miss distances for the aft rotors vary with the vehicle pitch. This is supported by the shift in noise reduction trends with thrust setting between the two vehicle orientations. Further investigations are warranted, both in terms of flow field visualizations of the rotor and airframe wakes as well as full vehicle flight testing to verify these potential acoustic benefits in a real-world setting.

ACKNOWLEDGMENTS

The authors would like to acknowledge John Swartzbaugh, Stanley Mason, Bryan Lamb, and Scott Parks of the LSAWT at NASA Langley Research Center for their tireless efforts involving facility test setup and data acquisition. This work was funded by the NASA Revolutionary Vertical Lift Technology (RVLT) project.

REFERENCES

[1] Patterson, M. Advanced Air Mobility (AAM): An Overview and Brief History. In *Transportation Engineering and Safety Conference*, Virtual Event, 2021. Available at: https://ntrs.nasa.gov/citations/20210024608.

[2] Diaz, P. V. and Yoon, S. Computational Study of NASA's Quadrotor Urban Air Taxi Concept. In *AIAA Scitech 2020 Forum*, AIAA Paper 2020-0302. Orlando, FL, January 2020.

[3] Christian, A. and Cabell, R. Initial Investigation into the Psychoacoustic Properties of Small Unmanned Aerial System Noise. In *23rd AIAA/CEAS Aeroacoustics Conference*, AIAA Paper 2017-4051. Denver, CO, June 2017.

[4] Rizzi, S. A., Zawodny, N. S., and Pettingill, N. A. On the use of Acoustic Wind Tunnel Data for the Simulation of sUAS Flyover Noise. In *25th AIAA/CEAS Aeroacoustics Conference*, AIAA Paper 2019-2630. Delft, The Netherlands, May 2019.

[5] Zawodny, N. S. and Pettingill, N. A. Acoustic Wind Tunnel Measurements of a Quadcopter in Hover and Forward Flight Conditions. In *Inter-Noise 2018*, pp. 487-500. Chicago, IL, August 2018.

[6] Zawodny, N. S. and Boyd, Jr., D. D. Investigation of Rotor-Airframe Interaction Noise Associated with Small-Scale Rotary-Wing Unmanned Aircraft Systems. *Journal of the American Helicopter Society*, **65(012007)**, 1–18 (2020).

[7] Pettingill, N. A. and Zawodny, N. S. Identification and Prediction of Broadband Noise for a Small Quadcopter. In *Vertical Flight Society 75th Annual Forum & Technology Display*, Philadelphia, PA, 2019.

[8] Zawodny, N. S. and Haskin, H. H. Small Propeller and Rotor Testing Capabilities of the NASA Langley Low Speed Aeroacoustic Wind Tunnel. In *23rd AIAA/CEAS Aeroacoustics Conference*, AIAA Paper 2017-3709. Denver, CO, June 2017.

[9] Zawodny, N. S., Boyd, Jr., D. D. and Burley, C. L. Acoustic Characterization and Prediction of Representative, Small-Scale Rotary-Wing Unmanned Aircraft System Components. In *AHS International* 72nd*Annual Forum*, West Palm Beach, FL, May 2016.

[10] Cadieux, F. Quadcopter Noise Prediction with the Lattice Boltzmann Method. In *Advanced Modeling and Simulation (AMS) Seminar Series*, Virtual Event, 2019. Available at: https://www.nas.nasa.gov/publications/ams/2019/12-18-19.html.

[11] Pettingill, N. A., Zawodny, N. S. and Thurman, C. S. Aeroacoustic Testing of UAS-Scale Rotors for a Quadcopter in Hover and Forward Flight. Submitted to *28th AIAA/CEAS Aeroacoustics Conference*. Southampton, UK, June 2022.

[12] Weitsman, D., Stephenson, J. H. and Zawodny, N. S. Effects of flow recirculation on acoustic and dynamic measurements of rotary-wing systems operating in closed anechoic chambers. *Journal of the Acoustical Society of America*, **148(3)**, 1325–1336 (2020).

[13] Whelchel, J., Alexander, W. N. and Intaratep, N. Propeller noise in confined anechoic and open environments. In *AIAA Scitech 2020 Forum*, AIAA Paper 2020-1252. Orlando, FL, January 2020.